Mineralogical Study of Lunar South Pole Region Using Chandrayaan-1 Hyperspectral (HySI) Data

R. Mohammed Zeeshan[1(✉)], B. Sayyad Shafiyoddin[1], R. R. Deshmukh[2], and Ajit Yadav[1]

[1] Department of Computer Science, Milliya Arts, Science and Management Science College, Beed 431122, Maharashtra, India
zeeeshan.shaikh@gmail.com, syedsb@rediffmail.com
[2] Department of Computer Science and IT, Dr. Babasaheb Ambedkar Marathwada University, Auranagabad, India
rrdeshmukh.csit@bamu.ac.in

Abstract. The main focus of the presented work was to better predict the surface mineralogy from the Chandrayaan-1 hyperspectral data set covering the area from South Pole region. To address the space weathering effect and to quantify mineralogy the Bi-directional reflectance function have been implemented. The implemented model was tested against two standard lunar laboratory mixtures and with the Apollo 10084 bulk soil sample. About 85 spectra were initially selected from varying locations and only active spectra with significant absorption were used for modeling. The minerals like plagioclase and Clinopyroxene were identified. Many spectra exhibits more iron content simulating mature area. Model result show no olivine content and very low Orthopyroxene content may be because of more crustal thickness, no impact would have penetrated to the lower mantle. Study reveals the potential of hyperspectral data multiplexed with mathematical model for not only mineral quantification but also helps to predict other associated parameters like grain size, iron fraction, phase function, however the spectra from mature soil and the limited HySI coverage acts as challenge for modelling process, modeling the data at longer wavelengths will be an advantage to improve the accurate mineral prediction.

Keywords: Hyperspectral · Absorption coefficient · Bi-directional reflectance

1 Introduction

The mineral analysis of the lunar surface using remotely sensed data from various lunar missions helps to understand the evolution and the composition of the moon [1].

The mineralogical study can be done by means of spatial analysis and spectral profile analysis. Creating the false color composite based on different band shaping algorithms like band strength band curve and band tilt is considered as standard spatial analysis technique [2, 3]. These band shaping algorithms was originally devised for UV-VIS

K. C. Santosh and B. Gawali (Eds.): RTIP2R 2020, CCIS 1381, pp. 163–175, 2021.
https://doi.org/10.1007/978-981-16-0493-5_15

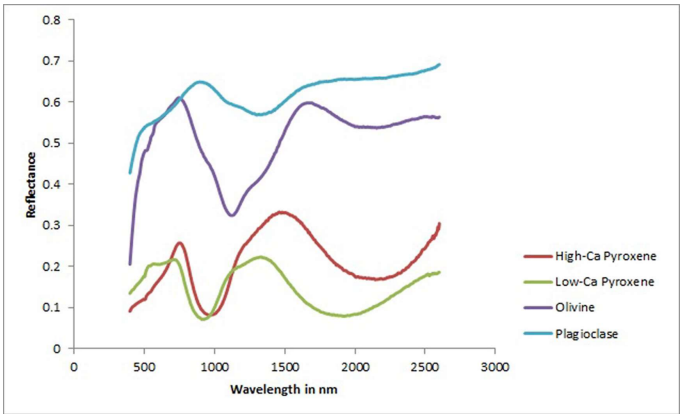

Fig. 1. Spectral signatures of common lunar minerals. (RELAB)

data to determine the surface mineralogy and later modified for HySI data as per HySI specifications [4]. The compositional variation using band parameters to identify different common lunar minerals like orthopyroxene, Clinopyroxene, olivine and Plagioclase were analyzed [5–8]. On the other hand the moon minerals can be well distinguished in the visible and near infrared part of the spectrum by its characteristic absorption features [9]. The chemical structure of the mineral causes change in shape, position and strength of the absorption band across the spectrum [10, 11]. The spectral profile analysis helps to study and identify different mineral from the lunar surface. Figure 1 shows the common major lunar minerals derived from RELAB database. Olivine, pyroxene and plagioclase are the common lunar minerals. The highland is Anorthositic in nature and it is mainly consists of plagioclase type of mineral with characteristic absorption at 1200 nm around ten percent of mafic component. From the Lunar return samples it is clear that for highland plagioclase is in between 15 to 75%. Whereas the low land area contains 10 to 35% of plagioclase. The second common mineral is from pyroxene group having characteristic absorption is at 1000 and 2000 nm with increasing amount of calcium the absorption shifts at the longer wavelengths. The shifts can clearly observe in Low-Ca pyroxene (Orthopyroxene) and High-Ca pyroxene (Clinopyroxene). The lunar soil contains 10 to 60% of pyroxene. The olivine type of mineral is having triplet absorption at 900, 1050 and 1250 nm. The lunar soil contains 2 to 15% of olivine.

2 Literature Review

The hyperspectral remotely sensed data provides a great opportunity to assess the mineralogy but the derived spectral signatures has great influence of an active mechanism that is consistently effects the lunar surface is termed as space weathering process. Space weathering involves two mechanisms firstly solar wind ion implantation and micro meteoritic bombardment [12, 13]. These two processes create a thin layer of submicroscopic iron (SMFe) which alters the spectral properties of soil and reflects strong influence on the spectra [14, 15]. Reduction in the overall reflectance, shallow absorption bands and red sloped continuum are the effects of space weathering on the spectra and can be observed in (Fig. 2). The hyperspectral moon mineralogy mapper (M3) data set onboard

Chandrayaan-1 with product id m3g20090104t161446_v01_rfl downloaded from PDS geosciences node lunar orbital data explorer (www.ode.rel.wustl.edu/moon) the extent of the area covers the mare crisium that is used to demonstrate the influence of space weathering. The red spectra derived from relatively fresh area appearing bright in the image and the blue spectra from mare area appearing dark. The red spectral profile has good spectral contrast as compared to blue spectra. As surface becomes mature it experiences more degree of space weathering accumulating more iron and hence reduces the spectral contrast which complicates the understanding of the surface mineralogy [16–19]. The space weathering effect acts as barrier for accurately assessing the surface mineralogy and compositional analysis. These effects can be address by means of a model based on theory of radiative transfer that best explains the space weathering effect on remotely sensed spectra. Three models are commonly used for modeling the remotely acquired spectra from airless bodies like moon are available. These models suitably describes the behavior of the electromagnetic radiation with the host material. The modified Gaussian model [20], Hapke's Bi-directional reflectance function based on fundamental equation of radiative transfer [21] and Shkuratov model [22]. The MGM model considers the absorption width, center and strength but as Chandrayaan-1 hyperspectral imager (HySI) data is used in this work, the spectral coverage of HySI act as constraint to use MGM model, whereas in Shkuratov model the viewing geometry is not included which greatly effects the reflectance pattern with change in geometry. On the other hand the Hapke's Bi-directional reflectance function that considers the host material as an intimate mixture and accommodates the effect of space weathering with other associated parameters [23–27]. The Hapke's model commonly used for modeling the remote spectra for mineral quantification [28–33].

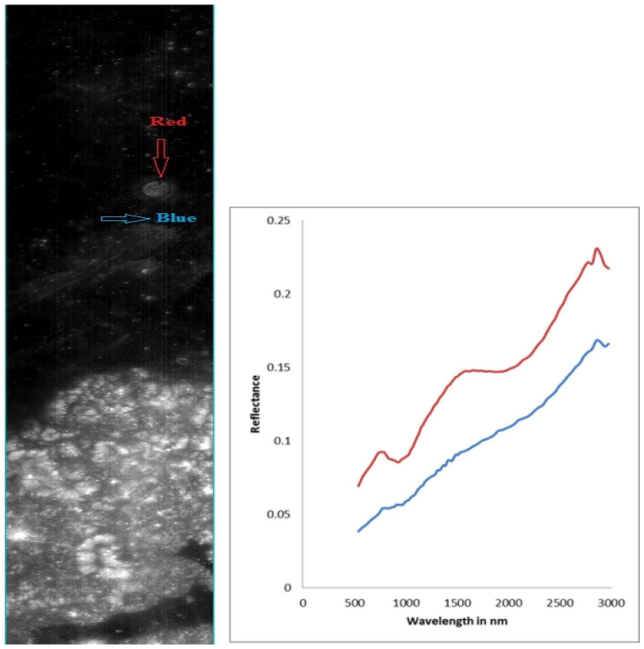

Fig. 2. Moon Mineralogy Mapper data set covering southern part of Mare Crisium and spectral profile from the highlighted areas.

3 Methodology

Modeled spectra or the hypothetical spectra is created for modeling the reflectance spectra derived from Chandrayaan-1 hyperspectral (HySI) data, the Bi-directional reflectance function is used and given by following Eq. (1). The five pure end member spectra of common lunar minerals are selected from RELAB database given (Fig. 3). Considering the spectral coverage of HySI from 0.43 μm to 0.96 μm the five end member is sufficient because within this spectral range most of the lunar mineral does not exhibit the absorptions and if we have data at longer wavelengths can only sense to take more end members for modeling process.

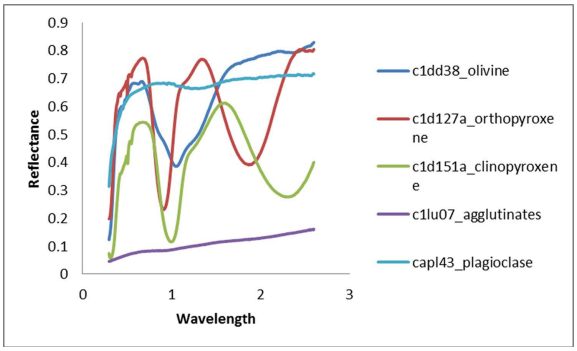

Fig. 3. The end member spectra used from RELAB database.

$$r_B = K\frac{w}{4\pi}\frac{\mu_0}{\mu_0+\mu}\left(\left[1+B(g)P(g)+H(\mu_0)H(\mu)-1\right)\right. \tag{1}$$

P (g) is phase function defines the angular scattering pattern of particles. *g* denotes phase angle, *B (g)* is opposition which is define as sudden bright spots that appears usually with small phase angles because of shadow-hiding and Chandrasekhar's H function accounts for multiple scattering part of the light. *w* is the single scattering albedo is the ratio of the scattering and extinction coefficient and need to be calculated first by Eq. (2) from [34]. The absorption coefficient of each end member is then calculated from Eq. 23(b) of [27] and it requires the real part of complex refractive index [35] as shown in (Fig. 4). The absorption coefficient of iron is derived using method from [27] which requires the complex refractive indices of iron taken from [36]. For introducing the space weathering effect into the model the absorption coefficient of end member and iron is added together and single scattering albedo was calculated.

The mixture is calculated by adding single scattering albedo of space weathered material given in Eq. (3) and requires specific density of each material end member taken from [35]. Finally the w_{im} substituted in Eq. (1) and remaining parameters like phase function for different angles, porosity parameter for different filling factors, and Chandrasekhar's parameters are calculated and substituted. Parameter study by considering each parameter and in combination of different parameters is carried and found that every parameter is working according to model definitions. The parameters like grain size, porosity, and phase function, iron fraction with different mass fractions of

minerals used to increase or decrease the spectral contrast of the modeled spectra. To increase the spectral contrast of modeled spectra, decrease grain size, decrease porosity, increase value of phase function, increase high albedo mineral like plagioclase, decrease iron content will result in overall increased spectral contrast and adding low albedo mineral like agglutinate, increasing grain size, increase porosity and adding more iron fraction which has the effect of space weathering results in decreased spectral contrast of the modeled spectra. After parameter study model validation is done using standard laboratory mixtures and with the Apollo 10084 bulk soil sample spectra.

$$W = 1 - \left(\frac{-27.856R + \sqrt{4.029R^2 + 602.932\mathrm{R} + 268.696\mathrm{R}}}{51.71R + 16.392} \right)^2 \tag{2}$$

$$w_{im} = \sum_{i=1}^{n} \frac{M(i)}{\rho(i)d(i)} w_{sw}(i) \Big/ \sum_{i=1}^{n} \frac{M(i)}{\rho(i)d(i)} \tag{3}$$

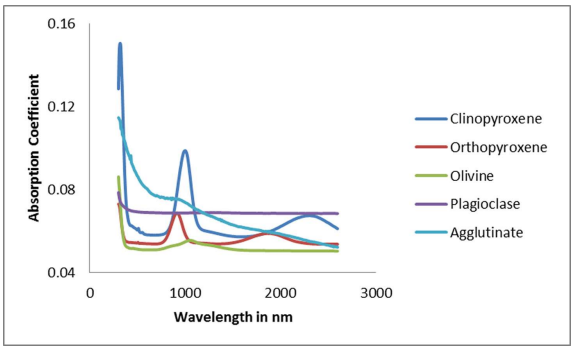

Fig. 4. The Derived Absorption coefficient of Selected end member.

3.1 Testing the Modeled Spectra

The artificial modeled spectra tested against the three components standard lunar mixtures by setting other parameters like grain size, phase function as average at 30° phase angle, 65% porosity and zero iron content means no space weathering effect for lab samples. Initially all mineral mass fractions and other parameters are set to lab specified values and it is found that the resultant modeled spectra is having close resemblance with the laboratory mixtures as shown in Fig. 5. For finding out the difference between measured and modeled spectra the mineral mass fractions is adjusted and it is observed that there is about 10% difference between measured lab spectra and modeled spectra. For the next test case the Apollo 10084 soil sample is used where the effect of space weathering is considered by adding iron fractions to the model and the mass fraction is set to the lab obtained values for the sample [37] and it is clearly observed from Fig. 5 that the model is successful in creating the actual trend in the spectra with 0.0005 of iron fraction. The laboratory mixture composition and composition of 10084 soil sample is given in Table 1. After model evaluation the spectra from the Chandrayaan-1 hyperspectral data set is derived and through modeling process mineralogy of the study area with particle size, iron fraction, porosity and function can be better predicted.

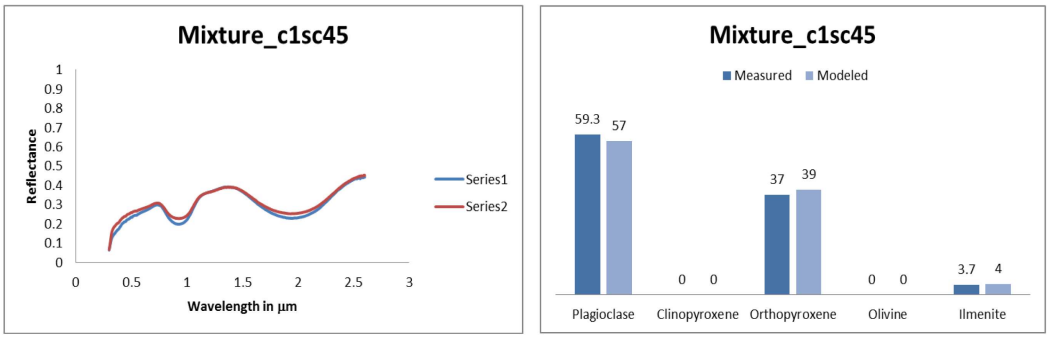

(a)

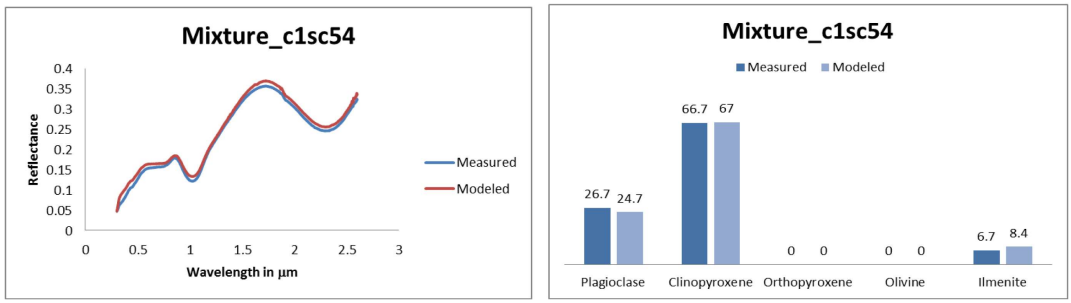

(b)

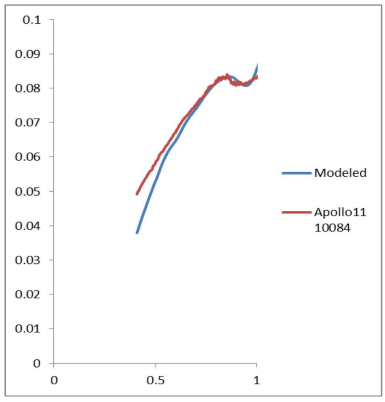

(c)

Fig. 5. **(a),** Measured and calculated modeled reflectance spectra of mixture c1sc45 and difference between measured and modeled composition. **(b),** Measured and Calculated Modeled reflectance spectra of mixture c1sc54 and Difference between Measured and Modeled Composition. **(c),** Measured and Modeled spectra of Apollo 10084 soil sample.

Table 1. Test mixture compositions

Mixture Id	Plagioclase	Clinopyroxene	Orthopyroxene	Ilmenite	Agglutinates	Source
C1sc45	59.3	0	37	3.7	0	RELAB
C1sc54	26.7	66.7	0	6.7	0	RELAB
10084	16.8	8.4	8.4	6.4	53.9	Morris 1978

4 Results and Discussion

The level-4 data product acquired by Chandrayaan-1 HySI instrument is used for analysing the surface minerals. The image cube is downloaded from the official website with product Id ending with 20090605T225556626. The image covering the area from south pole region close to Boguslawsky crater and it is also closed to proposed Chandrayaan-2 landing site near Mazinus and Simpelus craters is used. Figure 6 shows the extent of the study area and the actual HySI coverage with product id. The Hyper spectral imager (HySI) sensor acquires the data in pushbroom mode covering 430–964 nm having 64 continuous bands with the spectral resolution of 15 nm and spatial resolution of 80 m with 20 km swath [38].

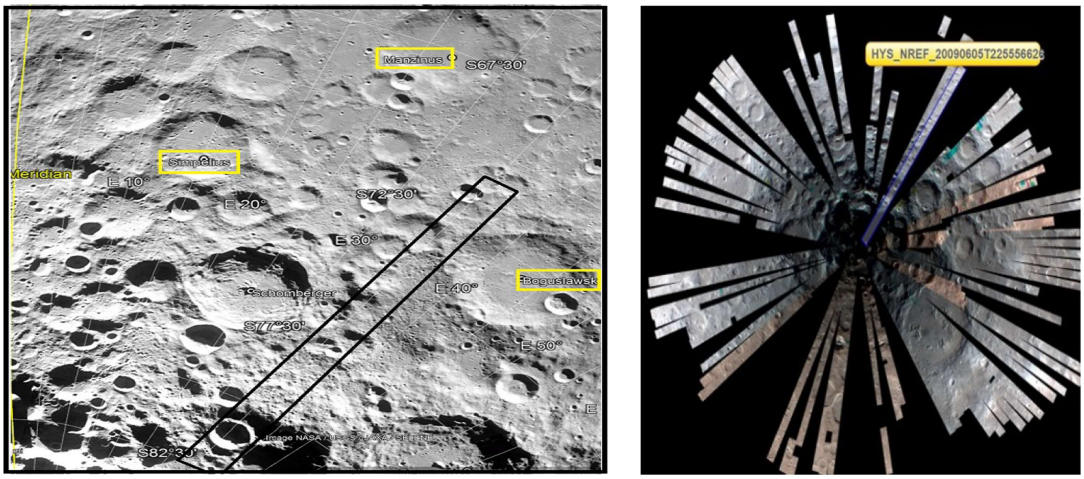

Fig. 6. South Pole map on google moon tool and extent of study area (left). Actual HySI South Pole coverage and highlighted study area.

The original data set is in radiance format and it is converted into reflectance image and divided into two parts. The Fig. 7 shows the subset of the study area with sampling site locations. The image is corrected and cross calibrated using 10084 Apollo bulk soil sample. Further the geometrical correction is performed using the geometry information provided with the data set. The region seems to be rugged and heavily craterd. For spectral profile analysis around 40 spectra from varying locations were selected. Most

of the spectra has no significant absorption and having red sloped continuum which indicates the high maturity of the area. However some 16 spectra selected from area appearing bright show adequate absorptions that can be suitable for modeling. These spectra are selected from the small young craters and from the crater walls of the large craters. The spectra from crater wall showing good reflectance with suitable band strength may be because of the gravitational slumping the material underneath getting exposed and these spectra are used for modeling. The spectral resolution of modeled spectra is 5 nm where as the Hysi spectral resolution is 15 nm so before modeling each Hysi spectra is interpolated to 5 nm and imported to the model routine.

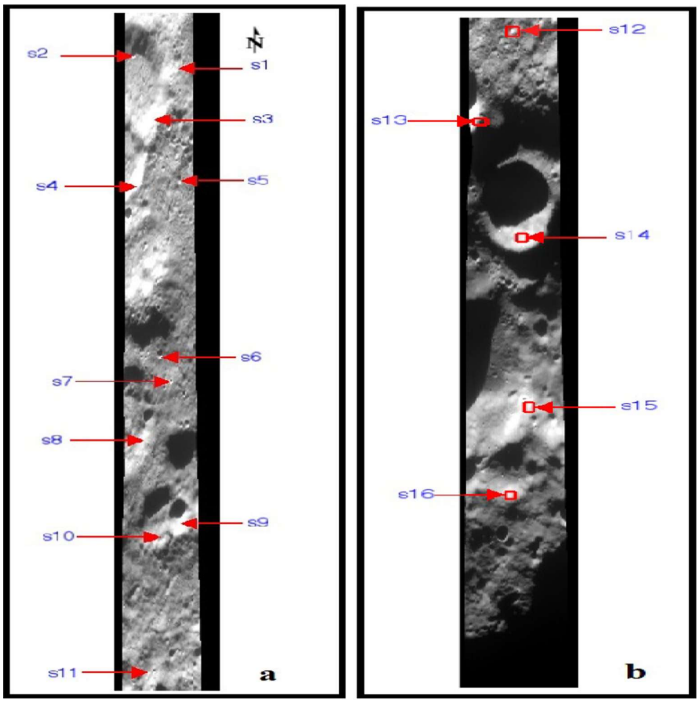

Fig. 7. Sampling Site Locations from the study area.

The Fig. 8 shows the reflectance spectra from the highlighted areas and the normalized spectra for better representation. The HySi spectral coverage is up to 964 nm so the modeled spectra are also clipped to 964 nm; both spectra are plotted into the same plot window. The spectra with no significant absorption and having very low reflectance is discarded from further process. Each spectra is modeled individually and the mineral mass fraction for each spectra is given in Table 2 and the parameter like grain size, porosity, iron fraction is given in Table 3. The spectra s7 shows the maximum reflectance around 21% with good absorption strength similarly spectra s4 and s13 is also showing good reflectance as they are extracted from the crater walls. The model results obtained for these spectra showing low iron mass fractions around 0.00015 with smaller grain size and showing 35 to 45% of Clinopyroxene with low percent of agglutinates with around 40% of plagioclase. The spectra s1 derived from northern part of the part (a) from Fig. 7 with low reflectance around 10% with complete absorption at 900 nm with 48% of orthopyroxene. About 11% low reflectance for spectra s16 shows mature soil with 0.00032 iron

fraction with 30% plagioclase and 37% Clinopyroxene and extracted from the crater wall. From modeling results no spectra shows olivine mineralogy may be it is lower mantle material so no impact would have penetrated through the crust to the lower mantle but here all representative spectra shows high values of Clinopyroxene may be the cratering event have penetrated to the upper mantle or the huge south pole Aitken event causes the material to spread around the south pole region. There are prominent rays scattered around the South Pole region form south pole Aitken. Figure 9 shows the sample measured and modeled spectra. The root mean square error and correlation coefficient used as a metric to measure the close resemblance of the measured and modeled spectra.

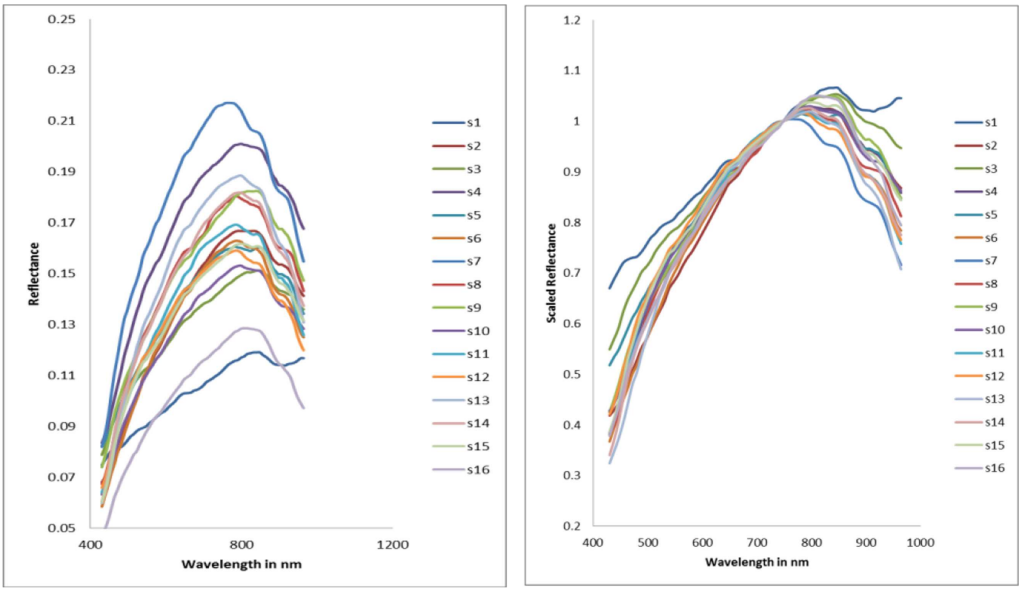

Fig. 8. Raw and Scaled reflectance spectra derived from the study area

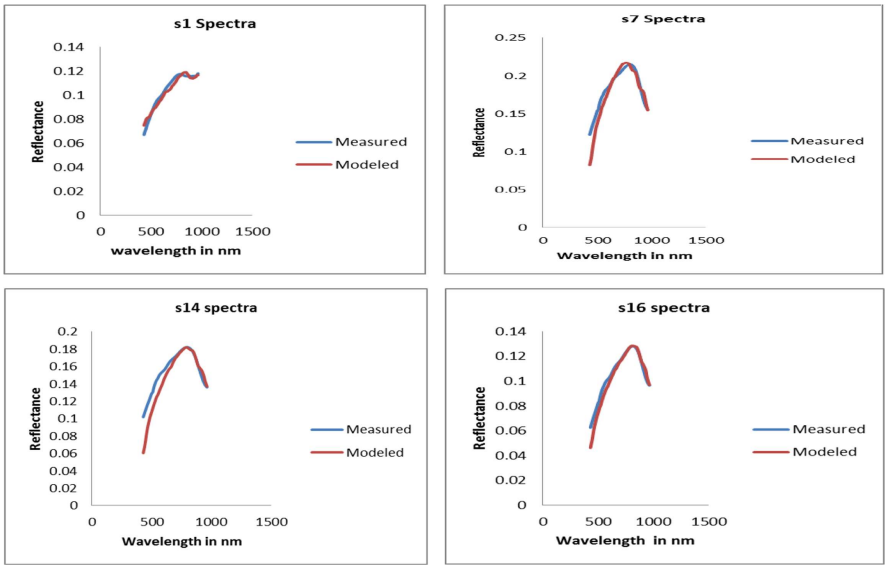

Fig. 9. Some sample measured spectra and modeled spectra from the study area.

Table 2. Mass fractions of each mineral obtained from the modeling process.

Spectra Id	Plagioclase	Clinopyroxene	Orthopyroxene	Olivine	Agglutinates
s1	31	0	48	0	21
s2	36	40	04	0	20
s3	36	36	0	0	28
s4	38	35	09	0	18
s5	33	35	12	0	20
s6	30	39	10	0	21
s7	42	44	0	0	14
s8	38	40	0	0	22
s9	37	39	03	0	21
s10	33	33	11	0	23
s11	30	38	05	0	16
s12	35	37	10	0	18
s13	33	40	10	0	15
s14	34	41	10	0	15
s15	33	35	07	5	24
s16	30	37	07	0	24

Table 3. The model parameters of each modeled spectra.

Spectra Id	Iron volume fraction	Average grain size (μm)	Porosity (%)	Phase function	Rmse	Correlation coefficient
s1	0.00026	63	60	average	0.0023	0.9874
s2	0.00026	99	60	average	0.0031	0.9903
s3	0.00031	108	60	average	0.0018	0.9967
s4	0.00016	86	60	average	0.0036	0.9923
s5	0.00025	113	60	average	0.0039	0.9920
s6	0.00025	98	60	average	0.0048	0.9843
s7	0.00015	51	60	average	0.0041	0.9832
s8	0.00029	94	60	average	0.0022	0.9981
s9	0.00029	85	60	average	0.0029	0.9953
s10	0.00029	87	60	average	0.0021	0.9935

(*continued*)

Table 3. (*continued*)

Spectra Id	Iron volume fraction	Average grain size (μm)	Porosity (%)	Phase function	Rmse	Correlation coefficient
s11	0.00023	88	60	average	0.0032	0.9921
s12	0.00023	88	60	average	0.0021	0.9982
s13	0.00015	92	60	average	0.0062	0.9482
s14	0.00018	93	60	average	0.0051	0.9676
s15	0.00023	78	59	average	0.0029	0.9949
z16	0.00032	75	66	average	0.0028	0.9938

5 Conclusion

The Chandrayaan-1 Hyperspectral data from south pole region near Chandrayaan-2 landing site is used for mineral analysis. The spectral profile analysis considering color composites based on different band parameters and spectral profile analysis is a standard technique for mineral mapping but for quantifying the mineralogy the radiative transfer model has been implemented for better prediction of mineralogical variation on the lunar surface. Moreover the space weathering process on an airless body like moon complicates and impedes the ability to get meaningful information hence the model also helps to determine the degree of space weathering in terms of iron fraction content. The results obtained from modeling process shows the high mass fraction of Clinopyroxne and low Orthopyroxene content for small fresh craters spread across the study area. The highland spectra shows high mass fraction for plagioclase. The mature spectra shows overall low reflectance and model return high iron content for such spectra with high agglutinates. The selected spectra shows around 40% of Clinopyroxene as spectra is selected from small young craters or either from crater wall having steep slopes. Spectra derived except the selected spectra showing very low reflectance with almost no absorption indicates very mature entire area hence difficult to model. At south pole region there is a strong chance of getting hydroxyl absorptions but the limited coverage of HySI dataset is constraint however data sets from other sensor with larger spectral coverage will gives an opportunity to model the spectra more accurately.

References

1. Jin, S., Arivazhagan, S., Araki, H.: New results and questions of lunar exploration from SELENE, Chang'E-1, Chandrayaan-1 and LRO/LCROSS. Adv. Space Res. **52**(2), 285–305 (2013)
2. McCord, T.B., Adams, J.B.: Progress in remote optical analysis of lunar surface composition. The Moon **7**(3–4), 453–474 (1973). https://doi.org/10.1007/BF00564646
3. Isaacson, P.J., Pieters, C.M.: Northern imbrium noritic anomaly. J. Geophys. Res. **114**, E09007 (2009). https://doi.org/10.1029/2008JE003293

4. Bhattacharya, S., Chauhan, P., Rajawat, A.S., Kumar, A.S.K.: Lithological mapping of central part of Mare Moscoviense using Chandrayaan-1 Hyperspectral Imager (HySI) data. Icarus **212**(2), 470–479 (2011). https://doi.org/10.1016/j.icarus.2011.02.006
5. Borst, A.M., Foing, B.H., Davies, G.R., van Westrenen, W.: Surface mineralogy and stratigraphy of the lunar south pole-Aitken basin determined from Clementine UV/VIS and NIR data. Planetary Space Sci. **68**(1), 76–85 (2012). https://doi.org/10.1016/j.pss.2011.07.020
6. Sayyad, S.B., Mohammed, Z.R., Deshmukh, R.R.: Mineral mapping of mare cresium using Chandrayaan-1 Hyperspectral (HySI) data. J. Appl. Sci. Comput. **5**(7), 88–95 (2018)
7. Sivakumar, V., Neelakantan, R.: Mineral mapping of lunar highland region using Moon Mineralogy Mapper (M3) hyperspectral data. J. Geol. Soc. India **86**(5), 513–518 (2015). https://doi.org/10.1007/s12594-015-0341-1
8. Sivakumar, V., Neelakantan, R., Santosh, M.: Lunar surface mineralogy using hyperspectral data: implications for primordial crust in the Earth-Moon system. Geosci. Front. **8**(3), 457–465 (2017). https://doi.org/10.1016/j.gsf.2016.03.005
9. Burns, R.G.: Mineralogical Applications of Crystal Field Theory. Cambridge University Press, New York (1970)
10. Anbazhagan, S., Arivazhagan, S.: Reflectance spectra of analog basalts; implications for remote sensing of lunar geology. Planet. Space Sci. **57**(12), 1346–1358 (2009)
11. Anbazhagan, S., Arivazhagan, S.: Reflectance spectra of analog anorthosites: Implications for lunar highland mapping. Planet. Space Sci. **58**(5), 752–760 (2010)
12. Hapke, B.: Effects of a simulated solar wind on the photometric properties of rocks and powders. Ann. N. Y. Acad. Sci. **123**, 711–721 (1965). https://doi.org/10.1111/j.1749-6632.1965.tb20395.x
13. Hapke, B.: Inferences from the optical properties of the moon concerning the nature and evolution of the lunar surface. Radio Sci. **5**, 293–299 (1970). https://doi.org/10.1029/RS005i002p00293
14. Hapke, B.: Darkening of silicate rock powders by solar wind sputtering. The Moon **7**, 342–355 (1973). https://doi.org/10.1007/BF00564639
15. Hapke, B., Cassidy, W., Well, E.: Effects of vapor-phase deposition processes on the optical, chemical, and magnetic properties of the lunar regolith. The Moon **13**,339–353 (1975). https://doi.org/10.1007/BF00567525
16. Keller, L.P., Mckay, D.S.: Discovery of vapor deposits in the lunar regolith. Science **261**, 1305–1307 (1993)
17. Keller, L.P., McKay, D.S.: the nature and origin of rims on lunar soil grains. Geochim. Cosmochim. Ac. **61**, 2331–2341 (1997)
18. Taylor, L.A., Pieters, C.M., Keller, L.P., Morris, R.V., McKay, D.S.: Lunar mare soils: space weathering and the major effects of surface-correlated nanophase Fe. J. Geophys. Res.-Planets **106**, 27985–27999 (2001)
19. Taylor, L. A., et al.: Mineralogical and chemical characterization of lunar highland soils: insights into the space weathering of soils on airless bodies, J. Geophys. Res. Planets **115**, E02002 (2010)
20. Sunshine, J.M., Pieters, C.M., Prait, S.F.: Deconvolution of mineral absorption bands: an improved approach. J. Geophys. Res. **95**(B5), 6955–6966 (1990). https://doi.org/10.1029/JB095iB05p06955
21. Hapke, B.: Bidirectional reflectance spectroscopy: I. Theory. J. Geophys. Res. Solid Earth **86**(B4), 3039–3054 (1981). https://doi.org/10.1029/JB086iB04p03039
22. Shkuratov, Y.G., Starukhina, L., Huffmann, H., Arnold, G.: A model of spectral albedo of particulate surfaces: implications for optical properties of the Moon. Icarus **137**(2), 235–246 (1999). https://doi.org/10.1006/icar.1998.6035
23. Hapke, B., Wells, E.: Bidirectional reflectance spectroscopy. II Experiments and observations. J. Geophys. Res. **86**, 3055–3060 (1981)

24. Hapke, B.: Bidirectional reflectance spectroscopy. III - Correction for Macroscopicroughness, Icarus **59**, 41–59 (1984)
25. Hapke, B.: Bidirectional reflectance spectroscopy IV - The extinction coefficient and the opposition effect. Icarus **67**(2), 264–280 (1986). https://doi.org/10.1016/0019-1035(86)90108-9
26. Hapke, B.: Theory of reflectance and emittance spectroscopy. Topics in Remote Sensing, Cambridge. Cambridge University Press, UK (1993)
27. Hapke, B.: Space weathering from Mercury to the asteroid belt. J. Geophys. Res. Planets **106**(E5), 10039–10073 (2001). https://doi.org/10.1029/2000JE001338
28. Clark, R.N., Roush, T.L.: Reflectance spectroscopy: quantitative analysis techniques for remote sensing applications. J. Geophys. Res. **89**, 6329–6340 (1984). https://doi.org/10.1029/JB089iB07p06329
29. Mustard, J.F., Pieters, C.M.: Quantitative abundance estimates from bidirectional reflectance measurements. In: Proceedings of the 17th Lunar and Planetary Science Conference, Part 2 (1987). J. Geophys. Res. **92**, E617–E626 (1987). https://doi.org/10.1029/JB092iB04p0E617
30. Lucey, P.G.: Mineral maps of the Moon. Geophys. Res. Lett. **31**, L08701 (2004). https://doi.org/10.1029/2003GL019406
31. Lawrence, S.J., Lucey, P.G.: Radiative transfer mixing models of meteoritic assemblages. J. Geophys. Res. **112**, E07005 (2007). https://doi.org/10.1029/2006JE002765
32. Cahill, J.T.S., Lucey, P.G., Wieczorek, M.A.: Compositional variations of the lunar crust: results from radiative transfer modeling of central peak spectra. J. Geophys. Res. **114**, E09001 (2009). https://doi.org/10.1029/2008JE003282
33. Cahill, J.T.S., Lucey, P.G., Stockstill-Cahill, K.R., Hawke, B.R.: Radiative transfer modeling of near-infrared reflectance of lunarhighland and mare soils. J. Geophys. Res. **115**, E12013 (2010). https://doi.org/10.1029/2009JE003500
34. Yan, B., Wang, R., Gan, F., Wang, Z.: Minerals mapping of the lunar surface with Clementine UVVIS/NIR data based on spectra un mixing method and Hapke model. Icarus **208**, 11–19 (2010)
35. Hiroi, T., Pieters, C.M.: Estimation of grain sizes and mixing ratios of fine powder mixtures of common geologic minerals. J. Geophys. Res. **99**(E5), 10867 (1994). https://doi.org/10.1029/94JE00841
36. Johnson, P.B., Cristy, R.W.: Optical constants of metals: Ti, V, Cr, Mn, Fe, Co, Ni, and Pd, prb. Phys. Rev. **9**, 5056–5070 (1974)
37. Morris, R.V.: The surface exposure /maturity/ of lunar soils - some concepts and Is/FeO compilation. In: Proceedings of the 9th Lunar and Planetary Science Conference, Houston, TX, 13–17 March 1987, vol. 2, pp. 2287–2297. Pergamon Press, Inc., New York (1978)
38. Kumar, A.: Hyper spectral imager for lunar mineral mapping in visible and near infrared band. Curr. Sci. **96**, 496 (2009)